ELSEVIER

Chemical Engineering Journal 140 (2008) 488–496

Chemical Engineering Journal

www.elsevier.com/locate/cej

Gas phase hydrogenation of maleic anhydride to tetrahydrofuran by $Cu/ZnO/TiO_2$ catalysts in the presence of *n*-butanol

Ruichao Zhang, Hengbo Yin *, Dongzhi Zhang, Lin Qi, Huihong Lu, Yutang Shen, Tingshun Jiang

Faculty of Chemistry and Chemical Engineering, Jiangsu University, Xuefu Road 301, Zhenjiang 212013, PR China

Received 21 September 2007; received in revised form 12 November 2007; accepted 26 November 2007

Abstract

$Cu/ZnO/TiO_2$ catalysts were prepared via the coprecipitation method. The catalysts were characterized by X-ray diffraction, X-ray photoelectron spectrometry, temperature programmed reduction, and N_2 adsorption. The catalytic activity of $Cu/ZnO/TiO_2$ catalyst in gas phase hydrogenation of maleic anhydride in the presence of *n*-butanol was studied at 235–280 °C and 1 MPa. The conversion of maleic anhydride was more than 95.7% and the selectivity of tetrahydrofuran was up to 92.7%. At the same time, *n*-butanol was converted to butyraldehyde and butyl butyrate via reactions, namely, dehydrogenation, disproportionation, and esterification. There were two kinds of CuO species present in the calcined $Cu/ZnO/TiO_2$ catalysts. At a lower copper content, the CuO species strongly interacted with ZnO and TiO_2; at a higher copper content, both the surface-anchored and bulk CuO species were present. The metallic copper (CuO) produced by the reduction of the surface-anchored CuO species favored the deep hydrogenation of maleic anhydride to tetrahydrofuran. The deep hydrogenation activity of $Cu/ZnO/TiO_2$ catalyst increased with the decrease of crystallite sizes of CuO and the increase of microstrain values. Compensations of reaction heat and H_2 in the coupling reaction of maleic anhydride hydrogenation and *n*-butanol dehydrogenation were distinct.

Keywords: Maleic anhydride; *n*-Butanol; Hydrogenation; Tetrahydrofuran; $Cu/ZnO/TiO_2$

1. Introduction

Tetrahydrofuran (THF) is widely used both as a versatile solvent and as a raw material for the manufacture of polytetramethylene ether glycol (PTMEG), spendex fibers, and polyurethane elastomers [1–3]. The majority of tetrahydrofuran is produced by the following two processes: the furfural process and the Reppe process [1,3]. In the former, possibly carcinogenic furfural is used as the raw material; in the latter, explosive acetylene and possibly carcinogenic formaldehyde are used as the feed stocks. On the other hand, the severe reaction conditions and multi-step reaction pathways also make the above-mentioned production processes unfavorable. To overcome the disadvantages of the established processes, eco-friendly and economically alternative process is worthy of investigation. A very promising alternative to the established processes is the single stage hydrogenation of maleic anhydride since maleic anhydride can be produced at a lower cost and on a large scale by partial oxidation of *n*-butane instead of benzene now [1,4–6].

Catalytic hydrogenation of maleic anhydride to succinic anhydride, γ-butyrolactone, 1,4-butanediol, and tetrahydrofuran has been an attractive research topic in the last decade since the hydrogenation products are important chemicals in the production of polymers, pharmaceuticals, and rubber additives, etc. [4,5,7,8]. Hydrogenation of maleic anhydride has been catalyzed by various kinds of catalysts, such as noble metals (Pd, Re, and Ru) in liquid phase at pressures between 1 and 5 MPa and temperatures between 190 and 240 °C [9–13], copper-based catalysts in liquid phase at pressures between 5 and 9 MPa and temperatures between 200 and 240 °C [7,9], and copper-based catalysts in gas phase at atmospheric pressure and temperatures between 210 and 280 °C [6,14,15]. The gas phase hydrogenation of maleic anhydride commonly used $Cu/ZnO/M_xO$ (Al, Cr, Ce, etc.) catalysts. During the above-mentioned researches, the high yield of γ-butyrolactone is generally achieved. However, tetrahydrofuran is usually produced with a lower yield and considered as a by-product.

* Corresponding author. Tel.: +86 511 88787591; fax: +86 511 88791800.
E-mail address: yin@ujs.edu.cn (H. Yin).

1385-8947/$ – see front matter © 2007 Elsevier B.V. All rights reserved.
doi:10.1016/j.cej.2007.11.031

To our best knowledge, there are no published papers dealing with the direct hydrogenation of maleic anhydride to tetrahydrofuran with a high yield except several patents [16,17]. Schlitter et al. [16] used Cu(Pd)/Al_2O_3 catalysts for gas phase hydrogenation of maleic anhydride to tetrahydrofuran, the yield of tetrahydrofuran was up to 93% at a reaction temperature of 250 °C and the pressures ranging from 0.1 to 2 MPa. Budge and Pedersen [17] used Cu/ZnO/Al_2O_3/Cr_2O_3 as a catalyst for the hydrogenation of maleic anhydride to tetrahydrofuran in the presence of monohydric aliphatic alcohol such as ethanol and butanol at the reaction temperatures between 200 and 325 °C and the pressures between 1.5 and 5.0 MPa, the yield of tetrahydrofuran was up to 99.1%. Other relative method for the preparation of tetrahydrofuran is the hydrogenation of the derivatives of maleic anhydride, e.g. Müller et al. [3] reported that dimethyl maleate or dimethyl succinate was converted to tetrahydrofuran by Cu/ZnO/Al_2O_3 catalyst at a reaction pressure of 2.5 MPa and a reaction temperature of 220 °C. In the Müller's process, an extra esterification process of maleic anhydride is needed before the catalytic hydrogenation, giving a multi-stage process for tetrahydrofuran production. The patented literatures reveal that it is possible to directly hydrogenate maleic anhydride to tetrahydrofuran with a high yield. But the presence of noble metal palladium and polluting chromium in the catalysts is unfavorable in view of both the catalyst cost and the environmental protection.

According to the literatures for the preparation of tetrahydrofuran from maleic anhydride or its derivatives [3,16,17], a common feature exists, i.e. the investigated catalysts are composed of metallic copper (CuO), ZnO, and Al_2O_3. In the catalytic hydrogenation process, it is commonly believed that CuO supplies hydrogenation active sites and that ZnO and Al_2O_3 play a role of support. For example, in the hydrogenation process of dimethyl maleic anhydride or dimethyl succinate to tetrahydrofuran, Müller et al. [3] suggested that Cu° catalyzes the hydrogenation and hydrogenolysis reactions yielding γ-butyrolactone and 1,4-butanediol and that Al_2O_3 provides weakly acidic sites to promote the subsequent dehydration of 1,4-butanediol to tetrahydrofuran. But Lu et al. [18] have recently reported that TiO_2 with acidic sites-modified Cu/Al_2O_3 catalyst was beneficial to the formation of γ-butyrolactone in the gas phase hydrogenation of maleic anhydride. The role of the supports is still at controversy.

It is well known that TiO_2 is a widely used material as a catalyst support or as a catalyst itself. It is reasonable to predict that TiO_2 as an alternative to Cr or Al present in copper-based catalyst should have a positive impact on the selective hydrogenation of maleic anhydride.

Recently, coupling of an exothermic hydrogenation reaction and an endothermic dehydrogenation reaction in one reaction system attracted researchers' interest in view of thermodynamics [19–21]. Copper-based catalysts can not only catalyze the

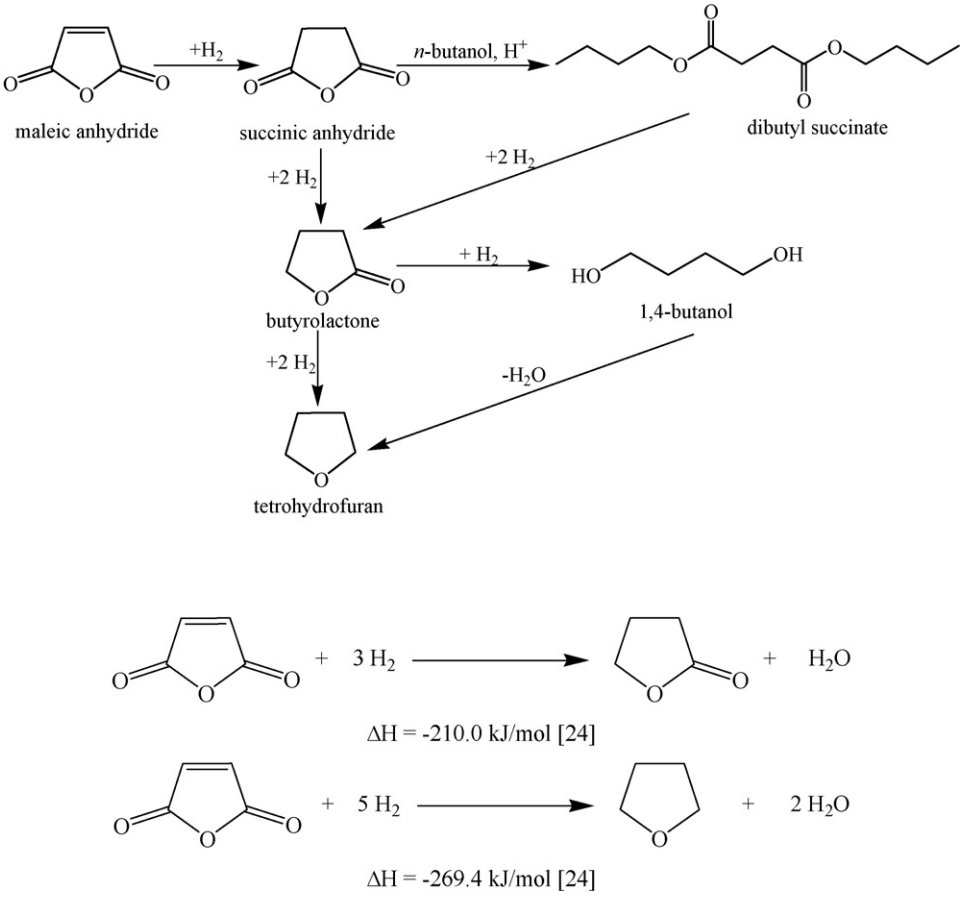

Scheme 1. Hydrogenation route of maleic anhydride [3,5,6,24].

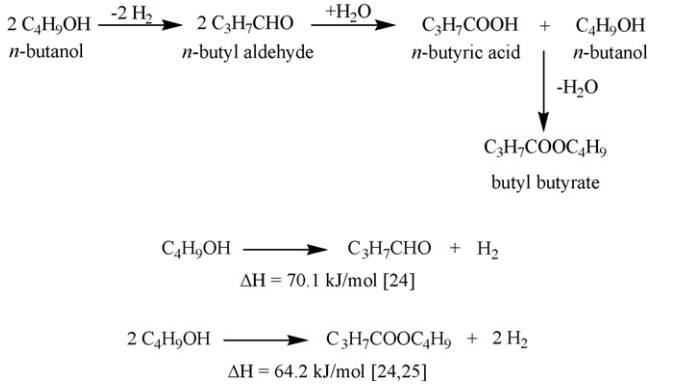

Scheme 2. Dehydrogenation route of *n*-butanol [6,22–25].

gas phase hydrogenation of maleic anhydride but also can catalyze the gas phase dehydrogenation of linear primary alcohols with *n* carbon atoms to corresponding valuable aldehyde and ester with 2*n* carbon atoms instead of the traditional esterification catalyst H_2SO_4 [22,23]. The hydrogenation of maleic anhydride and dehydrogenation of *n*-butanol are illustrated in Schemes 1 and 2 [3,5,6,22–25].

From Scheme 1, we found that producing 1 mol tetrahydrofuran requires 1 mol maleic anhydride and 5 mol H_2, releasing 269.4 kJ heat and that producing 1 mol γ-butyrolactone requires 1 mol maleic anhydride and 3 mol H_2, releasing 210.0 kJ heat. From Scheme 2, we found that producing 1 mol butyraldehyde requires 1 mol *n*-butanol, releasing 1 mol H_2 and requiring 70.1 kJ heat and that producing 1 mol butyl butyrate requires 2 mol *n*-butanol, releasing 2 mol H_2 and requiring 64.2 kJ heat. It can be predicated that the coupling of hydrogenation of maleic anhydride and dehydrogenation of a linear primary alcohol, such as *n*-butanol, in one reaction system using a copper-based catalyst should be beneficial to the two reactions in view of the compensations of H_2 and reaction heat.

In the present work, the hydrogenation of maleic anhydride catalyzed by Cu/ZnO/TiO_2 catalysts in the presence of *n*-butanol was carried out at a pressure of 1 MPa and the reaction temperatures ranging from 225 to 280 °C. The major objective of this work is to gain an insight into the catalytic activity of Cu/ZnO/TiO_2 catalysts in the hydrogenation of maleic anhydride to tetrahydrofuran and the dehydrogenation of *n*-butanol to butyraldehyde and butyl butyrate.

2. Experimental

2.1. Catalyst preparation

Cu/ZnO/TiO_2 catalysts were prepared via a continuous coprecipitation method. A mixed solution of $Cu(NO_3)_2{\cdot}3H_2O$, $Zn(NO_3)_2{\cdot}6H_2O$, and $TiCl_4$ with a given atomic ratio was used as a precursor solution and a Na_2CO_3 solution (1 M) was added as a precipitating agent. The coprecipitation was performed at 75 °C and the flow rates of the two solutions were adjusted to give a constant pH of ca. 8.5. The resultant precipitate was washed with distilled water until the conductivity of the filtrate was less than 2 mS/m, dried at 120 °C for 12 h, and then calcined at 350 °C for 2 h. The calcined catalysts were pressed at 24.5 MPa to form pellets and the pellets were crushed to form small-sized particles with particle sizes ranging from 0.4 to 0.8 mm for characterization by X-ray diffraction (XRD), X-ray photoelectron spectroscopy (XPS), temperature programmed reduction (TPR), nitrogen adsorption, and catalytic test. For XRD and XPS characterization of the H_2-reduced Cu/ZnO/TiO_2 catalysts, the calcined Cu/ZnO/TiO_2 catalysts were reduced under the same reduction procedure as described in the catalytic test section. The reduced Cu/ZnO/TiO_2 catalysts were cooled to ambient temperature in a N_2 stream and sealed in plastic bags before XRD and XPS characterization. The chemical composition of the prepared catalysts is illustrated in Table 1.

Table 1
The compositions, specific surface areas, and average pore diameters of the calcined Cu/ZnO/TiO_2 catalysts

Samples	Atomic ratios (Cu:Zn:Ti)	Specific surface areas (m^2/g)	Average pore diameters (nm)
C1	1:2:0.5	139.5	3.83
C2	1:2:1	172.9	3.83
C3	1:2:2	210.6	3.83
C4	2:2:1	148.9	3.40
C5	2:2:1.5	186.0	3.42
C6	2:2:2	186.3	3.41
C7	1:0:2	184.6	3.41
C8	2:2:0	38.3	7.77

2.2. Characterization

XRD analysis was used to examine the bulk structures of the calcined and reduced catalysts. The XRD data were recorded on a Rigaku D/Max-IIIB diffractometer using Cu Kα radiation (1.5418 Å) with Ni filter, scanning from 20° to 80° (2θ). Annealed strain-free KCl was measured by XRD from 20° to 80° in order to obtain instrumental contribution to broadening. The microstructure parameters, such as crystallite size (*D*) and microstrain value (ε) of the CuO (1 1 1) in the reduced catalysts, were calculated by the line-profile analysis based on the Voigt function [26]. The results are listed in Table 2.

XPS analyses of the calcined and reduced catalysts were recorded on a PHI-5300 ESCA spectrometer (PerkinElmer) using Mg Kα radiation (35.75 eV). The binding energies were calculated with respect to C1s peak at 285 eV with a precision of ±0.2 eV.

The reduction behaviors of the calcined catalysts were investigated by TPR technique using a mixed H_2/N_2 flow (10:90, v/v) of 50 ml/min and 20 mg of the calcined catalyst at a tempera-

Table 2
The crystallite sizes and microstrain values of metallic coppers (1 1 1) in the reduced Cu/ZnO/TiO_2 catalysts

	C1	C2	C3	C4	C5	C6	C7
D (nm)	19.4	11.5	12.0	17.8	15.3	20.8	77.2
ε ($\times10^{-3}$)	2.2	7.9	5.0	2.4	2.5	1.7	0.6

ture ramp of 10 °C/min from 25 to 400 °C. H_2 consumption was determined by analyzing the effluent gas with a thermal conductivity detector. The calcined samples were preheated in air at 300 °C before the TPR measurement in order to eliminate impurities and adsorbed water.

The specific surface areas and the average pore sizes of the calcined catalysts were measured on a NOVA 2000e physical adsorption apparatus and calculated with BET and BJH methods, respectively. The results are shown in Table 1.

2.3. Catalytic test

The catalytic test was carried out in a stainless steel tubular fixed-bed reactor with diameter and length of 8 and 200 mm, respectively, packed with 5 ml of catalyst with particle sizes ranging from 0.4 to 0.8 mm, operating at 235–280 °C and 1 MPa. The reactor was fed with a stream of maleic anhydride/*n*-butanol solution (12:88, w/w) in hydrogen, the liquid space velocity of maleic anhydride was 0.2 h^{-1}, and the molar ratio of H_2 to maleic anhydride was 50:1. The maleic anhydride/*n*-butanol solution was evaporated in an evaporator at 250 °C. Prior to the experiments, the catalysts were firstly reduced at atmospheric pressure in a mixed H_2/N_2 (10:90, v/v) stream with a flow rate of 250 ml/min from 25 to 200 °C at a temperature ramp of 1.5 °C/min and from 200–280 °C at a temperature ramp of 1.0 °C/min. Then the catalyst was continuously reduced at 280 °C for 2 h in a mixed H_2/N_2 (30:70, v/v) stream with a constant flow rate of 250 ml/min. After the reduction, the mixed gas was replaced by pure H_2 and the reaction pressure was raised to 1 MPa by adjusting pressure valves. The products were condensed by water bath and collected at the different reaction temperatures after reaction for 1 h. The collected reaction products were analyzed by using a gas chromatograph equipped with FID and a PEG packed capillary column (0.25 mm × 30 m). The experimental results are listed in Table 3.

Table 3
Activities of the Cu/ZnO/TiO_2 catalysts in maleic anhydride hydrogenation in the presence of *n*-butanol

Samples	*t* (°C)	X(MA) (%)	S (%)			X(BU) (%)	S (%)			H_2%	Heat%
			THF	GBL	DS		BA	BB	DS		
C1	280	97.5	75.9	24.1	0.0	18.3	24.3	75.7	0.0	40.4	29.6
	265	98.0	77.8	16.0	6.2	16.2	16.9	75.4	7.7	33.4	23.8
	250	97.5	59.2	27.7	13.1	13.5	14.7	65.8	19.5	27.6	19.4
	235	98.5	35.3	53.0	11.7	7.7	16.3	53.2	30.5	15.3	10.6
C2	280	97.3	81.5	18.5	0.0	18.0	20.5	79.5	0.0	39.0	27.9
	265	98.0	84.5	15.5	0.0	15.1	19.3	80.7	0.0	32.0	22.7
	250	98.5	73.8	24.8	1.4	11.0	17.8	79.6	2.6	23.7	16.4
C3	280	96.0	92.7	7.3	0.0	16.8	22.7	77.3	0.0	35.0	26.1
	265	97.8	92.3	7.7	0.0	13.7	20.8	79.3	0.0	28.3	20.7
	250	98.5	73.1	25.5	1.4	8.3	23.1	73.5	3.4	17.9	13.1
C4	280	97.0	78.7	21.3	0.0	17.6	23.5	76.5	0.0	38.7	28.3
	265	98.0	75.2	23.3	1.5	14.7	15.9	82.1	2.1	31.9	21.7
	250	99.0	56.8	41.8	1.4	11.7	15.4	82.2	2.4	27.3	17.7
	235	99.0	39.0	59.6	1.4	7.1	18.1	77.9	4.0	18.0	11.5
C5	280	97.0	81.1	18.9	0.0	16.6	26.2	73.8	0.0	36.0	27.1
	265	98.0	79.3	18.9	1.8	15.0	19.8	77.8	2.4	31.9	22.8
	250	98.5	55.0	36.8	8.2	11.4	18.7	66.8	14.5	24.6	17.4
	235	99.0	31.6	61.1	7.3	6.6	21.3	56.2	22.5	14.4	10.0
C6	280	97.0	83.5	16.5	0.0	18.6	20.6	79.4	0.0	40.0	28.8
	265	98.3	77.4	20.7	1.9	15.4	20.4	77.1	2.5	32.9	23.6
	250	98.5	48.8	39.0	12.2	11.5	18.2	60.4	21.4	24.0	17.2
	235	98.5	15.5	69.5	15.0	5.8	12.7	49.7	37.7	16.5	10.5
C7	280	96.0	0.0	14.7	85.3	19.2	11.8	0.8	87.4	19.0	–
	265	97.0	0.0	6.5	93.5	19.5	4.2	0.2	95.6	7.6	–
	250	97.0	0.0	0.0	100	20.2	1.5	0.0	98.5	3.0	–
	235	96.5	0.0	0.0	100	20.0	0.8	0.0	99.2	1.6	–
C8	280	96.2	13.4	74.0	12.6	16.3	5.4	81.3	13.3	28.7	–
	265	95.7	14.3	76.5	9.2	13.4	5.7	82.3	12	23.1	–
	250	96.4	10.1	77.1	12.8	10.0	3.9	75.8	20.3	18.0	–
	235	97.1	7.9	76.2	15.9	6.3	3.4	63.3	33.3	11.7	–

MA, maleic anhydride; THF, tetrahydrofuran; GBL, γ-butyrolactone; DS, dibutyl succinate; BU, *n*-butanol; BA, butyraldehyde; BB, butyl butyrate; X, conversion; S, selectivity. H_2% = (the amount of hydrogen produced in *n*-butanol dehydrogenation/the amount of hydrogen consumed in MA hydrogenation) × 100%. Heat% = (the heat consumed in the formation of butyraldehyde and butyl butyrate/the heat released in the formation of γ-butyrolactone and tetrahydrofuran) × 100%, calculated at standard state (25 °C, 0.1 MPa).

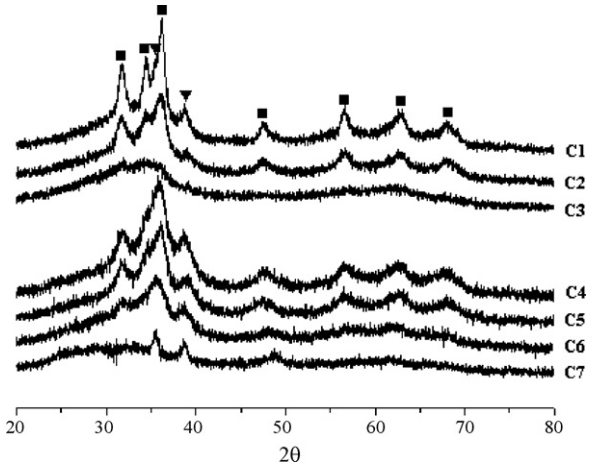

Fig. 1. XRD patterns of the calcined Cu/ZnO/TiO_2 catalysts. (▼) CuO; (■) ZnO.

3. Results and discussion

3.1. Characterization of Cu/ZnO/TiO_2 catalysts

3.1.1. XRD analysis

The XRD patterns of the calcined and reduced Cu/ZnO/TiO_2 catalysts are shown in Figs. 1 and 2. The XRD patterns of the calcined Cu/ZnO/TiO_2 catalysts exhibit the characteristic peaks of CuO (PDF#48-1548) and ZnO (PDF#36-1451), appearing at $2\theta = 35.5°$, 38.7°, 31.8°, 34.4°, 36.3°, 47.5°, 56.6°, 62.9°, 68.0°, respectively. The characteristic peaks of TiO_2 were not detected in the calcined Cu/ZnO/TiO_2 catalysts, revealing that TiO_2 should be present in an amorphous phase. The XRD patterns of the reduced Cu/ZnO/TiO_2 catalysts show that CuO was reduced to CuO (PDF#04-0836) with characteristic peaks appearing at $2\theta = 43.3°$, 50.4°, and 74.1°, and that zinc species were still present in the form of ZnO. After reduction, there was no characteristic peak of TiO_2 detected by XRD analysis, meaning that TiO_2 was still present in the amorphous phase.

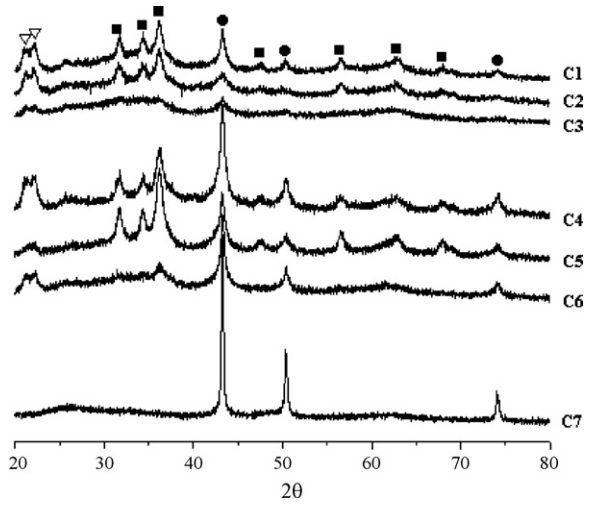

Fig. 2. XRD patterns of the reduced Cu/ZnO/TiO_2 catalysts. (●) CuO; (■) ZnO; (▽) SiO_2 arising from the quartz wool pad under catalyst in reactor.

As far as the reduced catalysts are concerned, the crystallite sizes (D) and the microstrain values (ε) of metallic copper (1 1 1) were estimated according to the line-profile analysis based on the Voigt function. For the Cu/ZnO/TiO_2 catalysts (C1–C6), the crystallite sizes of metallic copper were between 11.5 and 20.8 nm, and the range of their microstrain values was from 1.7×10^{-3} to 7.9×10^{-3}. For the Cu/TiO_2 catalyst (C7), the crystallite size of metallic copper was much larger up to 77.2 nm, and the microstrain value decreased to 0.6×10^{-3}. The presence of ZnO enables the crystallite size of metallic copper to decrease, while the microstrain value to increase, meaning that the dispersivity of metallic copper is enhanced and the lattice distortion is increased by ZnO.

3.1.2. XPS analysis

The chemical states of the representative calcined Cu/ZnO/TiO_2 (C2), calcined Cu/TiO_2 (C7), and H_2-reduced Cu/ZnO/TiO_2 (C2) catalysts were evaluated by XPS. Fig. 3 shows the Cu2p3/2 and Cu2p1/2 peaks of the calcined and H_2-reduced samples. The calcined samples C2 and C7 displayed the principal Cu2p3/2 and Cu2p1/2 peaks at 932.8, 952.8; 933.4, 953.1 eV, respectively, when referenced to the C1s core level at 285 eV, which is characteristic of Cu^{2+} species [27,28]. Furthermore, the presence of Cu^{2+} satellite peak appearing at 942 eV evidenced the presence of Cu^{2+} ions in the form of cupric oxide, although whose origin is complex and has been explained as due to electron shake-up processes, final state effects, and charge transfer mechanisms [28]. The binding energies of Cu2p3/2 and Cu2p1/2 of Cu/TiO_2 (C7) catalyst shifted to higher values than that of Cu/ZnO/TiO_2 catalyst (C2), revealing that the chemical state of CuO is influenced by the composition of the catalyst.

The binding energies of Ti2p3/2 and Ti2p1/2 of the calcined Cu/TiO_2 (C7) and Cu/ZnO/TiO_2 (C2) catalysts were 458.4, 463.9; 458.3, 464 eV, respectively, pertaining to that of TiO_2 [29].

After reduction with H_2, the Cu2p3/2 and Cu2p1/2 of Cu/ZnO/TiO_2 catalyst (C2) shifted to lower binding energy at ca. 931.6 and 951.6 eV and the satellite peak disappeared, meaning that after reduction the copper species are Cu^+ or Cu°, rather than Cu^{2+} [27,30]. The shift of Cu2p3/2 alone reveals the disappearance of cupric oxide, but does not allow to reach a conclusion about the presence of solely cuprous oxide or solely metallic copper or both since the Cu2p3/2 peaks for metallic copper and Cu_2O appear with the same binding energy. But the appearance of Cu2p1/2 at 951.6 eV as well as the disappearance of the satellite peak at ca. 942 eV can be ascribed to the formation of metallic copper rather than cuprous copper as certified by Mayanna and co-workers [28]. Furthermore, the XRD patterns of the reduced samples only show the existence of metallic copper for copper species. Therefore, it can be concluded that CuO present in the calcined samples is reduced to CuO under the present experimental conditions.

3.1.3. TPR analysis

The temperature programmed reduction curves of the calcined samples are shown in Fig. 4. For the Cu/TiO_2 catalyst (C7),

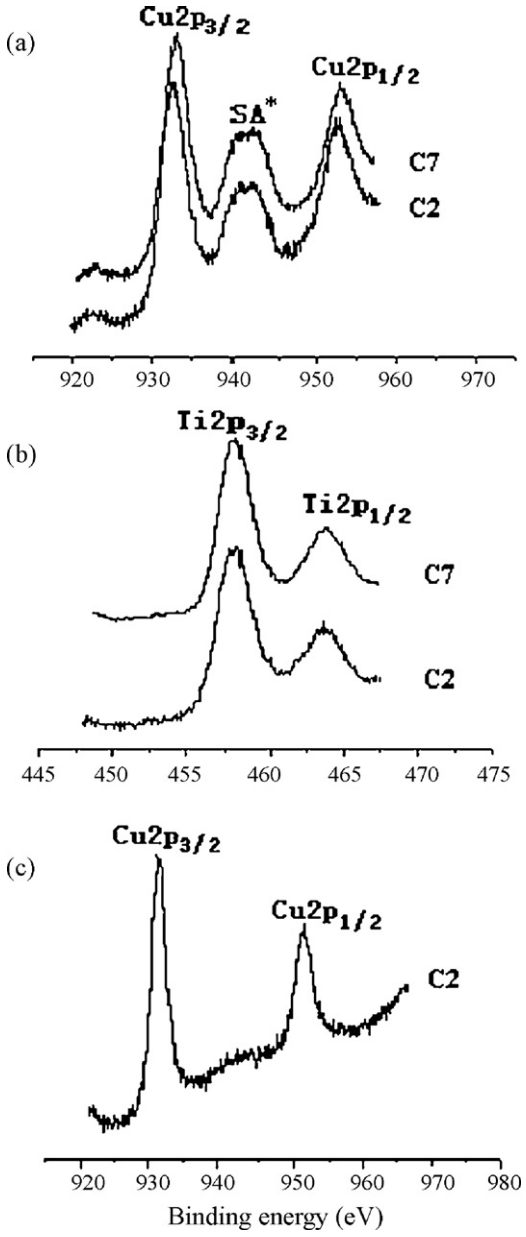

Fig. 3. X-ray photoelectron spectra of the representative calcined and H_2-reduced catalysts. (a and b) Calcined C2 and C7 samples; (c) reduced C2 sample.

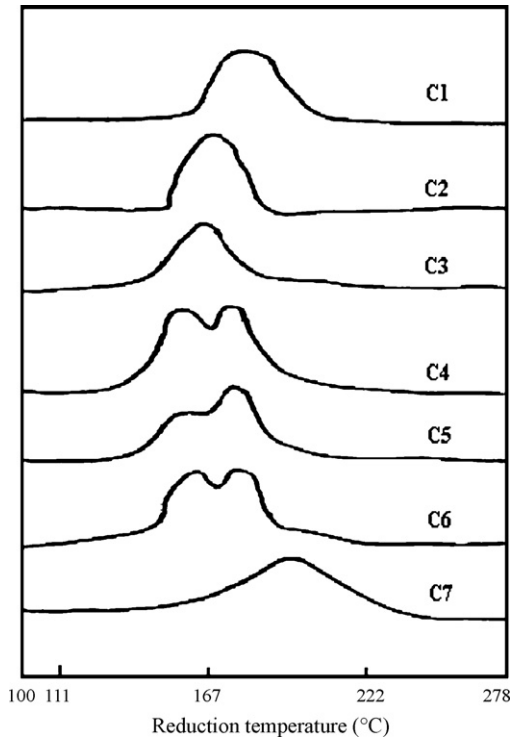

Fig. 4. TPR profiles of the Cu/ZnO/TiO_2 catalysts.

the TPR peak was broad and the maximum TPR peak appeared at 190.8 °C, higher than those of all the Cu/ZnO/TiO_2 catalysts. Reduction of Cu/TiO_2 catalyst at a higher temperature could be explained as being due to the fact that the interaction between CuO and TiO_2 in Cu/TiO_2 catalyst inhibited the reduction of CuO.

For Cu/ZnO/TiO_2 catalysts (C1–C3) with a lower copper content (Cu:Zn:Ti, 1:2:0.5–2), a single TPR peak for each sample was detected, and the temperatures at the maximum peaks shifted from 177.8 °C to a lower temperature of 165 °C with increasing the TiO_2 content. From XPS analysis, we found that the binding energies of Cu2p3/2 and Cu2p1/2 of the Cu/ZnO/TiO_2 catalyst (C2) shifted to lower values than those for the Cu/TiO_2 (C7) catalyst, meaning that the presence of ZnO in Cu/ZnO/TiO_2 catalyst influenced the interaction between CuO and TiO_2. Therefore, the shift of the TPR peaks toward lower temperature with increasing the TiO_2 content in Cu/ZnO/TiO_2 catalysts could be explained as being due to the fact that the chemical state of CuO was synergistically affected by both ZnO and TiO_2.

With the increase of the CuO content in Cu/ZnO/TiO_2 catalysts (C4–C6, Cu:Zn:Ti, 2:2:1–2), the TPR curves for all the tested catalysts exhibited two peaks at the temperatures ranging from 154.1 to 157.8 °C and from 168.7 to 179.8 °C, respectively. The TPR peaks appearing at higher temperature should be ascribed to the reduction of the surface-anchored CuO, i.e. the CuO strongly interacted with ZnO and TiO_2, since the temperatures at the maximum peaks are within the same range as those of the Cu/ZnO/TiO_2 catalysts with a lower CuO content (samples C1–C3). On the other hand, the TPR peaks appearing at lower temperature should be ascribed to the reduction of the bulk CuO present in the Cu/ZnO/TiO_2 catalysts.

3.1.4. Specific surface area and average pore size analysis

The specific surface areas and average pore sizes of the Cu/ZnO/TiO_2, Cu/ZnO, and Cu/TiO_2 catalysts are listed in Table 1. The specific surface areas of the Cu/ZnO/TiO_2 and Cu/TiO_2 catalysts are more than 139.5 m^2/g, revealing that the catalysts containing TiO_2 can provide high surface areas. The range of the average pore sizes of the Cu/ZnO/TiO_2 and Cu/TiO_2 catalysts is from 3.4 to 3.83 nm. The pore sizes are appropriate for the catalytic characteristics of maleic anhydride hydrogenation [31]. However, the Cu/ZnO catalyst has a small specific surface area and a large average pore size. Therefore,

the presence of TiO_2 is beneficial to the increasing of the specific surface area of the catalyst.

3.2. Catalysis results

3.2.1. Hydrogenation of maleic anhydride

Table 3 shows the catalytic activities of the Cu/ZnO/TiO_2 catalysts (C1–C6) for maleic anhydride hydrogenation and *n*-butanol dehydrogenation at 1 MPa and 235 to 280 °C. The experimental results show that the conversion of maleic anhydride was more than 96% under the present reaction conditions, the selectivity of tetrahydrofuran was more than 75%, up to 92.7%, at the high reaction temperature of 265 or 280 °C, and γ-butyrolactone and dibutyl succinate were the other hydrogenation products of maleic anhydride. As shown in Table 3, the selectivity of tetrahydrofuran increased with elevating reaction temperature, while the selectivities of γ-butyrolactone and dibutyl succinate decreased. The catalytic hydrogenation of maleic anhydride by copper-based catalyst proceeds via consecutive hydrogenation steps, in which succinic anhydride, γ-butyrolactone, 1,4-butanediol, and tetrahydrofuran are formed subsequently. The resultant succinic anhydride can react with the solvent, *n*-butanol, to produce dibutyl succinate [6]. Therefore, in hydrogenation of maleic anhydride to tetrahydrofuran, dibutyl succinate and γ-butyrolactone can be regarded as the intermediate products and tetrahydrofuran as the deep hydrogenation product. Since the conversion of maleic anhydride was close to 100%, the selectivity of tetrahydrofuran can be used as a criterion for evaluating the deep hydrogenation activity and the selectivity of dibutyl succinate as a criterion for evaluating the hydrogenation activity at a comparable conversion of maleic anhydride [6].

For Cu/ZnO/TiO_2 catalysts (C1–C3) with a low copper content (Cu:Zn:Ti, 1:2:0.5–2), the catalysts C2 and C3 exhibited much higher selectivity of tetrahydrofuran than C1 did and the maximum value was up to 92.7% (C3, 280 °C). Moreover, the selectivities of γ-butyrolactone and dibutyl succinate of the catalysts C2 and C3 were low, especially for the dibutyl succinate, whose selectivity was only 1.4%. By comparing the selectivities of the hydrogenation products, we found that at a lower copper content, the hydrogenation activity of Cu/ZnO/TiO_2 catalysts increased with increasing the content of TiO_2.

For Cu/ZnO/TiO_2 catalysts (C4–C6) with a high copper content (Cu:Zn:Ti, 2:2:1–2), the highest selectivity of tetrahydrofuran was up to 83.5%. The selectivities of tetrahydrofuran and γ-butyrolactone of the samples C4–C6 were comparable at the high reaction temperatures ranging from 250 to 280 °C. However, at a low reaction temperature of 235 °C, the selectivity of tetrahydrofuran decreased and the selectivity of γ-butyrolactone increased with increasing the content of TiO_2. Furthermore, the selectivity of dibutyl succinate increased with increasing TiO_2 content.

For Cu/TiO_2 catalyst (C7; Cu:Ti, 1:2), dibutyl succinate with a selectivity of more than 85% was dominantly produced at the reaction temperatures between 235 and 280 °C, and small amount of γ-butyrolactone with a selectivity less than 15% was produced at the high reaction temperatures between 265 and 280 °C. Tetrahydrofuran as a deep hydrogenation product was not detected over Cu/TiO_2 catalyst. For Cu/ZnO catalyst (C8; Cu:Zn, 2:2), the selectivity of γ-butyrolactone was more than 74% and the selectivity of tetrahydrofuran was less than 14.3% at the reaction temperatures between 235 and 280 °C. The main hydrogenation product was γ-butyrolactone, instead of tetrahydrofuran. The selectivity of tetrahydrofuran catalyzed by Cu/ZnO/TiO_2 catalyst was higher than that by Cu/TiO_2 or Cu/ZnO catalyst. At the same time, the selectivity of dibutyl succinate catalyzed by Cu/ZnO/TiO_2 catalyst was lower than that by Cu/TiO_2 or Cu/ZnO catalyst. Therefore, it is reasonable to conclude that ZnO and TiO_2 present in the Cu/ZnO/TiO_2 catalysts have a synergistic effect on the promotion of the hydrogenation activity.

By comparing the selectivities of tetrahydrofuran, γ-butyrolactone, and dibutyl succinate at the comparable conversions of maleic anhydride, the hydrogenation activities of C1–C7 are in an order of C3 > C2 > C4 > C5 > C1 > C6 ≫ C7. Interestingly, the microstrain values of CuO in the reduced C1–C7 are in an order of C2 > C3 > C5 > C4 > C1 > C6 ≫ C7 and the crystallite sizes of CuO in the reduced C1–C7 are in the reverse order of the microstrain values (Table 2). The activity order of catalysts C1–C7 is roughly consistent with the order of the microstrain values of CuO. Therefore, it is reasonable to indicate that the hydrogenation activity increases with increasing the lattice distortion degree of CuO and decreasing crystallite size of CuO.

Although the lower copper-contented C1 had a little lower hydrogenation activity than the higher copper-contented C4 and C5 did, the hydrogenation activity of C1 was comparable to that of C4 and C5 and higher than that of C6. Furthermore, the lower copper-contented C2 and C3 had obviously higher hydrogenation activity than the higher copper-contented C4–C6 did. According to the TPR analysis, we found that CuO species were anchored at the surfaces of ZnO and TiO_2 at a lower copper content and that both surface-anchored and bulk CuO species were present at a higher copper content. Therefore, it is reasonable to suggest that CuO originating from the surface-anchored CuO should have higher catalytic activity than that originating from the bulk CuO in hydrogenation of maleic anhydride.

3.2.2. Reaction route of maleic anhydride hydrogenation catalyzed by Cu/ZnO/TiO_2 catalyst

Considering that the conversion of maleic anhydride was close to 100% in the most cases, we suggested that the C=C bond present in maleic anhydride is easily hydrogenated by Cu/ZnO/TiO_2 catalysts at 1 MPa and the temperatures ranging from 235 to 280 °C. However, there was no succinic anhydride but γ-butyrolactone and dibutyl succinate with a large scale produced at the lower reaction temperature, and the selectivity of γ-butyrolactone was higher than that of dibutyl succinate. Hence it can be concluded that the hydrogenation of the resultant succinate anhydride to γ-butyrolactone is a fast process and that the esterification between succinate anhydride and *n*-butanol is a slow process. It is well known that dibutyl succinate can be hydrogenated to γ-butyrolactone. Under the present reaction conditions, only a small amount of dibutyl succinate was formed

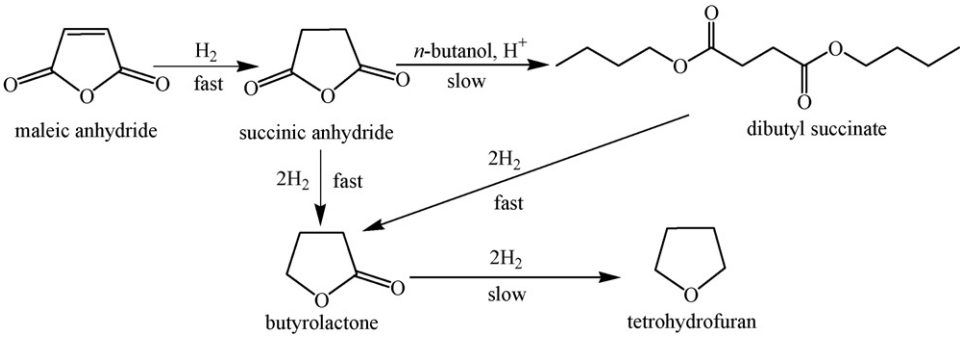

Scheme 3. Reaction route of maleic anhydride hydrogenation catalyzed by Cu/ZnO/TiO_2 catalysts.

at the lower reaction temperature, meaning that the hydrogenation of dibutyl succinate to γ-butyrolactone should be a rapid process.

The selectivity of γ-butyrolactone is larger than that of tetrahydrofuran when the temperature is 235 °C. However, the selectivity of γ-butyrolactone decreased rapidly with elevating reaction temperature from 235 to 280 °C, accompanied by the rapid increase of the selectivity of tetrahydrofuran. Tetrahydrofuran should be mainly produced by the hydrogenation of γ-butyrolactone. Since higher selectivity of tetrahydrofuran was obtained at the higher temperature, i.e. the much severe reaction condition was needed for the formation of tetrahydrofuran, it can be concluded that the hydrogenation of γ-butyrolactone to tetrahydrofuran is a slow process.

According to the above discussions, we suggested a reaction route of maleic anhydride hydrogenation catalyzed by Cu/ZnO/TiO_2 catalysts as shown in Scheme 3.

3.2.3. Dehydrogenation of n-butanol

The dehydrogenation process of *n*-butanol by copper-based catalysts can be illustrated in Scheme 2 [6,22,23]. In the dehydrogenation process, *n*-butanol is firstly dehydrogenated to form butyraldehyde; the resultant butyraldehyde is converted to butyric acid and *n*-butanol via a disproportionation reaction; then the resultant butyric acid and *n*-butanol is converted to butyl butyrate via an esterification reaction.

Table 3 shows the dehydrogenation–disproportionation–esterification results of *n*-butanol over a series of catalysts (C1–C7) at 1 MPa and 235 to 280 °C. For Cu/ZnO/TiO_2 catalysts (C1–C6), the conversions of *n*-butanol increased (in a range of 5.8–18.6%) as elevating the reaction temperature from 235 to 280 °C. In general, the selectivities of butyraldehyde and butyl butyrate increased as elevating the reaction temperature from 235 to 280 °C, ranging from 12.7 to 26.2% and 49.7 to 82.2%, respectively. Although the conversions of *n*-butanol catalyzed by Cu/ZnO/TiO_2 catalysts (C1–C6) at the same reaction temperature are close to each other, but the selectivities of dibutyl succinate are in an order of C2 < C3 < C4 < C5 < C1 < C6 when *n*-butanol is taken as the key reactant. Considering that the products starting from *n*-butanol only consist of butyraldehyde, butyl butyrate, and dibutyl succinate, it is reasonable to conclude that the order of *n*-butanol dehydrogenation activities of the Cu/ZnO/TiO_2 catalysts (C1–C6) is C2 > C3 > C4 > C5 > C1 > C6, similar to that of their maleic anhydride hydrogenation activities. It is worth noting that butyric acid as an intermediate product was not detected in the dehydrogenation process. This result reveals that the esterification between the resultant butyric acid and *n*-butanol is rapid.

For Cu/TiO_2 catalyst (C7), the conversion of *n*-butanol was ca. 20% at the reaction temperatures ranging from 235 to 280 °C, and the dominant product was dibutyl succinate. A small amount of butyraldehyde was produced at the reaction temperatures ranging from 235 to 280 °C and a trace of butyl butyrate was only produced at the high reaction temperatures of 265 and 280 °C. The dehydrogenation activity of Cu/TiO_2 catalyst is lower than that of Cu/ZnO/TiO_2 catalysts.

For Cu/ZnO catalyst (C8), the conversions of *n*-butanol were increased from 6.3 to 16.3% when the reaction temperatures were increased from 235 to 280 °C. The dominant product was butyl butyrate with the selectivities ranging from 63.3 to 82.3%. The conversion of *n*-butanol catalyzed by Cu/ZnO catalyst is slightly lower than that catalyzed by Cu/ZnO/TiO_2 catalysts. On the other hand, the selectivity of dibutyl succinate produced by the esterification of *n*-butanol and succinic anhydride is generally higher than that catalyzed by Cu/ZnO/TiO_2 catalysts. Therefore, the dehydrogenation activity of Cu/ZnO catalyst is lower than that of Cu/ZnO/TiO_2 catalysts. The coexistence of TiO_2 and ZnO in the Cu/ZnO/TiO_2 catalysts favors both the hydrogenation of maleic anhydride and the dehydrogenation of *n*-butanol.

3.2.4. Reaction route of n-butanol dehydrogenation catalyzed by Cu/ZnO/TiO_2 catalyst

As discussed above, a reaction route of *n*-butanol dehydrogenation by Cu/ZnO/TiO_2 catalyst was suggested as shown in Scheme 4.

The reactions of *n*-butanol dehydrogenation to butyraldehyde and butyraldehyde disproportion to butyric acid and *n*-butanol are slow processes. However, the esterification between butyric acid and *n*-butanol to butyl butyrate is a fast process.

3.2.5. Compensation between the hydrogenation and the dehydrogenation

Hydrogen produced by the dehydrogenation of *n*-butanol can be used as a feed stock for the hydrogenation of maleic

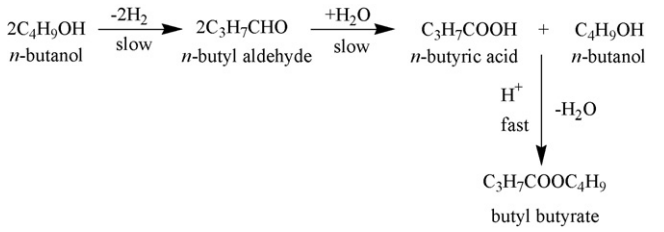

Scheme 4. Reaction route of *n*-butanol dehydrogenation by Cu/ZnO/TiO_2 catalysts.

anhydride. The ratios of the hydrogen produced in *n*-butanol dehydrogenation to the hydrogen consumed in maleic anhydride hydrogenation (H_2%) were calculated according to Schemes 3 and 4 and listed in Table 3. In the coupling process of hydrogenation and dehydrogenation catalyzed by Cu/ZnO/TiO_2 catalysts (C1–C6), the H_2% values increased with elevating reaction temperature from 235 to 280 °C and the H_2% values are in a range of 14.4–40.4%. On the other hand, in the coupling process catalyzed by Cu/TiO_2 catalyst (C7), the H_2% values increased from 1.6 to 19% with elevating the reaction temperature from 235 to 280 °C. For the Cu/ZnO catalyst, the H_2% values increased from 11.7 to 28.7% with elevating the reaction temperature from 235 to 280 °C. Therefore, Cu/ZnO/TiO_2 catalysts favor the H_2 compensation in the coupling process.

The heat produced by the exothermic hydrogenation of maleic anhydride can be transferred to the endothermic dehydrogenation of *n*-butanol. The ratios of the standard reaction heat absorbed by *n*-butanol dehydrogenation to the standard reaction heat released by maleic anhydride hydrogenation (Heat%) were calculated according to Schemes 1 and 2 and listed in Table 3. In the coupling process catalyzed by Cu/ZnO/TiO_2 catalysts (C1–C6), the Heat% values increased with elevating the reaction temperature from 235 to 280 °C in a range of 10–29.6%. It is evident that Cu/ZnO/TiO_2 catalysts favor the heat compensation in the coupling process.

4. Conclusions

For calcined Cu/ZnO/TiO_2 catalysts, at a lower copper content, the CuO species strongly interacted with ZnO and TiO_2; at a higher copper content, both the surface-anchored and bulk CuO species were present. The small-sized CuO with high microstrain values favored maleic anhydride hydrogenation. The CuO originating from the surface-anchored CuO species had a higher catalytic activity for hydrogenation of maleic anhydride to tetrahydrofuran than that originating from bulk CuO species. Cu/ZnO/TiO_2 catalysts had a higher activity for the dehydrogenation of *n*-butanol to butyraldehyde and butyl butyrate than Cu/TiO_2 and Cu/ZnO catalysts. CuO catalyzed the dehydrogenation of *n*-butanol to butyraldehyde and the disproportionation of the resultant butyraldehyde to butyric acid and *n*-butanol. The dehydrogenation of *n*-butanol supplied 14.4–40.4% H_2 which was consumed in the hydrogenation of maleic anhydride under the present experimental conditions over Cu/ZnO/TiO_2 catalysts. When the reaction heat was calculated at a standard state (25 °C, 0.1 MPa), the dehydrogenation of *n*-butanol consumed 10–29.6% reaction heat, which was released in the hydrogenation of maleic anhydride.

Acknowledgements

The work was financially supported by Jiangsu Province, China (1631310002) and Zhenjiang Science and Technology Bureau (GJ2006006). Authors sincerely thank Professor Yongfa Zhu at Tsinghua University for XPS measurement and Professor Kangmin Chen at Jiangsu University for XRD measurement.

References

[1] J. Kanetaka, T. Asano, S. Masamune, Ind. Eng. Chem. 62 (1970) 24.
[2] V. Pallassana, M. Neurock, G. Coulston, Catal. Today 50 (1999) 589.
[3] S.P. Müller, M. Kucher, C. Ohlinger, B. Kraushaar-Czarnetzkyi, J. Catal. 218 (2003) 419.
[4] A. Küksal, E. Klemm, G. Emig, Appl. Catal. A: Gen. 228 (2002) 237.
[5] S.G. Girol, T. Strunskus, M. Muhler, C. Wöll, J. Phys. Chem. B 108 (2004) 13736.
[6] T.J. Hu, H.B. Yin, R.C. Zhang, H.X. Wu, T.S. Jiang, Y. Wada, Catal. Commun. 8 (2007) 193.
[7] U. Herrmann, G. Emig, Ind. Eng. Chem. Res. 37 (1998) 759.
[8] A. Cybulski, J. Chrzaszcz, M.V. Twigg, Catal. Today 69 (2001) 241.
[9] U. Herrmann, G. Emig, Ind. Eng. Chem. Res. 36 (1997) 2885.
[10] S.M. Jung, E. Godard, S.Y. Jung, K.C. Park, J.U. Choi, J. Mol. Catal. A 198 (2003) 297.
[11] S.M. Jung, E. Godard, S.Y. Jung, K.C. Park, J.U. Choi, Catal. Today 87 (2003) 171.
[12] P. Liu, K. Yan, Y. Liu, Y. Yin, J. Nat. Gas Chem. 8 (1999) 157.
[13] Y. Hara, H. Kusaka, H. Inagaki, K. Takahashi, K. Wada, J. Catal. 194 (2000) 188.
[14] G.L. Castiglioni, A. Vaccari, G. Fierro, M. Inversi, M. Lo Jacono, G. Minelli, I. Pettiti, P. Porta, M. Gazzano, Appl. Catal. A: Gen. 123 (1995) 123.
[15] G.L. Castiglioni, M. Ferrari, A. Guercio, A. Vaccari, R. Lancia, C. Fumagalli, Catal. Today 27 (1996) 181.
[16] S. Schlitter, H. Borchert, M. Hesse, M. Schubert, N. Bottke, R. Fischers, M. Rosch, G. Heydrich, A. Weck, US 20,040,198,596A1 (2004).
[17] J.R. Budge, S.E. Pedersen, US 4,810,807 (1989).
[18] W. Lu, G. Lu, Y. Guo, Y. Guo, Y. Wang, Catal. Commun. 4 (2003) 177.
[19] Y.L. Zhu, J. Yang, G.Q. Dong, H.Y. Zheng, H.H. Zhang, H.W. Xiang, Y.W. Li, Appl. Catal. B: Environ. 57 (2005) 183.
[20] M.E.E. Abashar, Chem. Eng. Process. 43 (2004) 1195.
[21] J. Yang, H.Y. Zheng, Y.L. Zhu, G.W. Zhao, C.H. Zhang, B.T. Teng, H.W. Xiang, Y. Li, Catal. Commun. 5 (2004) 505.
[22] D.J. Elliott, F. Pennella, J. Catal. 119 (1989) 359.
[23] H.J. Wang, Q.W. Duan, Spec. Petrochem. (Chin.) 1 (2003) 20.
[24] R.L. David (Ed.), CRC Handbook of Chemistry and Physics, 85th ed., CRC Press, Baca Raton, 2005, p. 884.
[25] NIST Chemistry WebBook, NIST Standard Reference Database Number 69, June 2005 Release.
[26] L.S. Chen, G.L. Lu, Acta Chim. Sinica 53 (1995) 966.
[27] R.T. Figueiredo, A. Martinez-Arias, M.L. Granados, L.G. Fierro, J. Catal. 178 (1998) 146.
[28] C.L. Aravinda, P. Bera, V. Jayaram, A.K. Sharma, S.M. Mayanna, Mater. Res. Bull. 37 (2002) 397.
[29] J.C. Dupin, D. Gonbeau, I. Martin-litas, P. Vinatier, A. Levasseur, Appl. Surf. Sci. 173 (2001) 140.
[30] G. Mankowski, J.P. Duthil, A. Giusti, Corros. Sci. 39 (1997) 27.
[31] J. Li, Y. Jiang, J.Y. Cheng, H.M. Wang, Chin. J. Appl. Chem. 17 (2000) 379.